CMB signal in $WMAP$ **3yr data with** FASTICA

D. Maino[1][*], S. Donzelli[1], A. J. Banday[2], F. Stivoli[3], C. Baccigalupi[3,4]

[1] *Dipartimento di Fisica, Università di Milano, Via Celoria 16, I-20133, Milano, Italy*
[2] *Max-Planck Institute für Astrophysik, Karl-Schwarzschild Str. 1, D-85740, Garching, Germany*
[3] *SISSA/ISAS, Astrophysics Sector, Via Beirut 4, I-34014, Trieste*
[4] *INFN, sezione di Trieste, Via Valerio 2, I-34127, Trieste, Italy*

11 September 2006

ABSTRACT

We present an application of the fast Independent Component Analysis (FASTICA) to the $WMAP$ 3yr data with the goal of extracting the CMB signal. We evaluate the confidence of our results by means of Monte Carlo simulations including CMB, foreground contaminations and instrumental noise specific of each $WMAP$ frequency band. We perform a complete analysis involving all or a subset of the $WMAP$ channels in order to select the optimal combination for CMB extraction, using the frequency scaling of the reconstructed component as a figure of merit. We found that the combination KQVW provides the best CMB frequency scaling, indicating that the low frequency foreground contamination in Q, V and W bands is better traced by the emission in the K band.

The CMB angular power spectrum is recovered up to the degree scale, it is consistent within errors for all $WMAP$ channel combination considered, and in close agreement with the $WMAP$ 3yr results.

We perform a statistical analysis of the recovered CMB pattern, and confirm the sky asymmetry reported in several previous works with independent techniques.

Key words: methods – data analysis – techniques: image processing – cosmic microwave background.

1 INTRODUCTION

The Cosmic Microwave Background (CMB) anisotropies are at present the main tracer of the physical processes occurred in the very early universe; a complete mapping of them may reveal crucial clues about the statistics of the primordial perturbations, the existence of gravity waves, the global geometry of the universe as well as the physical components responsible for the accelerated expansion eras in the very early and recent universe, known as inflation and dark energy, respectively.

For these reasons, a great experimental work is being carried out in order to measure the finest structure of the CMB anisotropies. In total intensity, right after successful sub-orbital observations, the Wilkinson Microwave Anisotropy Probe ($WMAP$) satellite is performing all sky observations of the CMB in five frequency bands ranging between 22 and 90 GHz (see Spergel et al. 2006 and references therein). The first detections of the CMB polarization have been made from the ground (Kovac et al. 2002), balloons (Montroy et al. 2005) as well as from the $WMAP$ satellite itself (Page et al. 2006). In a few years the PLANCK satellite[1] will be launched, performing all sky measurements of the CMB total intensity and polarization anisotropy in 9 frequency bands between 30 and 857 GHz, with an angular resolution reaching 5 arcminutes with a sensitivity of a few micro-Kelvin. Next generation sub-orbital and satellite observations are ongoing or planned[2].

The observations are confirming that the Galactic and extra-Galactic foreground emissions represent one of the two most challenging obstacles to the complete knowledge of CMB anisotropies. The other one is represented by the control of instrumental systematics. In total intensity the sky at high Galactic latitudes appears dominated by the CMB emission at least

---

[*] E-mail: davide.maino@mi.infn.it
[1] http://www.rssd.esa.int/Planck
[2] http://lambda.gsfc.nasa.gov/

in the frequency range between 60 and 90 GHz observed by $WMAP$, although residual foreground contamination might be responsible for the deviations of the observed signal from a Gaussian statistics (see Copi et al. (2006) and references therein). In polarization the sky remains foreground dominated even if the region containing the brightest Galactic emission is cut out (Page et al. 2006). In particular, foregrounds are likely to be comparable or higher to the the curl component in the CMB polarization at all frequencies, and in any region of the sky (Baccigalupi 2003).

For these reasons it is important to study and test data analysis algorithms which are able to remove foreground contamination from the data. The class of these tools is called component separation, and they all make use of the multi-frequency superposition of the background and foreground emissions in order to separate them out. The concepts and means they use, however, are very different. The category of non-blind methods uses prior knowledge of the foreground emission in order to recover the CMB component (Brandt et al. 1994; Termark & Efstathiou 1996; Hobson et al. 1998; Bouchet et al. 1999; Barreiro et al. 2004; Stolyarov et al. 2005). Blind methods exploit the statistical independence between background and foregrounds. Among them, the Independent Component Analysis (ICA, see Amari & Chichocki 1998, and references therein) has provided interesting results on simulated data in total intensity (Baccigalupi et al. 2000; Maino et al. 2002) and polarization (Baccigalupi et al. 2004; Stivoli et al. 2006), as well as on the real data by $COBE$-DMR (Maino et al. 2003) and $BEAST$ (Donzelli et al. 2006); these results are based on an implementation of the ICA technique capable to rapidly achieve convergence to the solution if the hypothesis of statistical independence among the signals is verified (FASTICA Hyvärinen 1999). Recently, hybrids techniques merging the blind and non-blind categories and largely based on a parametric description of the foreground emission have been proposed (Delabrouille et al. 2003; Patanchon et al. 2005; Eriksen et al. 2006).

As we already mentioned, the design and testing of the component separation algorithms has been successful on real data. This, together with the results presented here, indicates that these techniques may become standard data analysis techniques, complementary to the methods of CMB extraction exploited so far. In this work we apply the FASTICA algorithm to the total intensity $WMAP$ 3yr data. Our purpose is to identify the CMB among the separated components and study its pattern in comparison with the findings of other works exploiting different techniques. The paper is organized as follows. In Section 2 we outline the main features of the FASTICA algorithm. In Section 3 we evaluate its capabilities on simulated $WMAP$ data. In Section 4 we apply the FASTICA to the $WMAP$ data and study the recovered CMB. Finally, in Section 5 we draw our conclusions.

2 COMPONENT SEPARATION PROBLEM

We report here a brief description of the FASTICA algorithm, focusing on how the data are modeled and its principal assumptions. For further details we refer to the original theoretical papers in signal processing (Hyvärinen 1999; Hyvärinen & Oja 2000) and to the CMB applications, in total intensity (Maino et al. 2002) and polarization (Baccigalupi et al. 2004).

Let us suppose that the sky radiation at a given frequency ν is the superposition of N different physical processes and that frequency and spatial dependencies can be factorized into two separated terms:

$$\tilde{x}(\boldsymbol{r}, \nu) = \sum_{j=1}^{N} \bar{s}_j(\boldsymbol{r}) f_j(\nu) \,. \tag{1}$$

By definition, and without loss of generality, the f functions may be defined to be 1 at a given reference frequency. In this case the signals s represent the actual emissions at that frequency. In order to exploit the different spectral behavior of CMB and foreground emissions, an M-frequencies experiment is usually exploited. Individual detectors are also coupled with an optical system, whose beam pattern is in general modeled, at each frequency, as a position invariant point spread function (PSF) $B(\boldsymbol{r}, \nu)$. In addition any real experiment adds instrumental noise $\epsilon_\nu(\boldsymbol{r})$ in the output signal. Indicating with $\nu_1, ..., \nu_M$ the M frequencies of a given experiment, one can define the scaling coefficients $a_{ij} = f_j(\nu_i)$, and construct the $M \times N$ mixing matrix $\mathbf{A}$ accordingly. Within these assumptions the observed signal is expressed by

$$\mathbf{x}(\boldsymbol{r}) = \mathbf{A}\bar{\mathbf{s}}(\boldsymbol{r}) * B(\boldsymbol{r}) + \boldsymbol{\epsilon}(\boldsymbol{r}) = \mathbf{A}\mathbf{s}(\boldsymbol{r}) + \boldsymbol{\epsilon}(\boldsymbol{r}) \,, \tag{2}$$

where for each position r, $\mathbf{x}$ and ϵ are vectors with M rows, and the star represents the convolution of the PSF with the sky signals $\bar{\mathbf{s}}$, indicated simply as $\mathbf{s}$ afterward; note that we further assumed that the beam function is frequency independent i.e. the signals at different frequencies are smoothed at the same angular resolution.

The problem is solved obtaining both the mixing matrix $\mathbf{A}$ and the signals $\mathbf{s}$ from the observed data $\mathbf{x}$. In the ICA approach, the lack of determination in the problem is compensated by assuming that the signals to recover are random realizations of independent distributions: this means that the joint probability distribution of the superposition is a product of the single ones for each signal; in particular this implies that all of them, but at most one, have non-Gaussian distributions. The actual separation is achieved by means of linear combinations of the input data at different frequencies, corresponding to the maxima of a suitable neg-entropy approximation and thus of the non-Gaussianity. The maxima are in the form of vectors $\mathbf{w}$, rows of the separation matrix $\mathbf{W}$ such that the transformed variables $\mathbf{y} = \mathbf{W}\mathbf{x}$ are indeed independent components. The

neg-entropy approximation is achieved by a non-linear re-mapping of the input data (Hyvärinen 1999; Hyvärinen & Oja 2000) exploiting suitably functions g, i.e. $g(u) = u^3$, $g(u) = \tanh(u)$ and $g(u) = u\exp(-u^2)$ where u are the principal component projected data. In the following these functions will be indicated as p, t and g. It is not possible to decide a priori which function will work better on a given data set: this indeed depends on the statistics of the independent signals which are not known a priori. In particular p, which corresponds to the kurtosis, should be used for sub-Gaussian components but it is strongly sensitive to outliers in the distributions; g is for super-Gaussian signals while t is a general purpose function (Hyvärinen 1999). Therefore this optimization step is something that have to be verified on a case-by-case basis. Similarly to previous works, in the application to the $WMAP$ data we have verified that best performances are obtained with g and we present results obtained with this function only.

Once the separation matrix $\mathbf{W}$ is obtained the underlying components are given by $\mathbf{x} = \mathbf{W}^{-1}\mathbf{y}$. This equation allows us to derive the frequency scalings for each independent component (Maino et al. 2002): the scaling between ν and ν' of the jth component is given by the ratio of $W_{\nu j}^{-1}/W_{\nu' j}^{-1}$. This ratio is directly related to the spectral index of the frequency spectrum of the component which, for a power law behavior, is written as $\beta = \log[W_{\nu j}^{-1}/W_{\nu' j}^{-1}]/\log[\nu/\nu']$.

The signal-to-noise ratio for the reconstructed components can also be recovered, as the noise enters into the separation process through the noise covariance $\mathbf{\Sigma}$ (Hyvärinen & Oja 2000). Therefore, noise constrained realization $\mathbf{n_x}$ for each frequency channels can be built and combined accordingly to the weights obtained by the separation matrix $\mathbf{W}$. This is exactly what we have done for evaluating the noise angular power spectrum in the recovered CMB component, as it was done for the FASTICA application to the $COBE$-DMR and $BEAST$ data Maino et al. (2003); Donzelli et al. (2006).

3 CALIBRATION WITH SIMULATIONS AND IDEAL PERFORMANCES

In order to construct an expectation of the results we obtain when applying FASTICA to the $WMAP$ 3yr data, we first tested the algorithm by means of Monte Carlo (MC) simulations. These give hints on performances in ideal situation and could be used, when compared to results from real data, to judge the accuracy of sky and instrument model adopted.

3.1 Simulation pipeline

We created synthetic skies at the 5 $WMAP$ frequency bands (23, 33, 41, 61 and 94 GHz) including instrumental noise and smoothed with a Gaussian beam of 1 degree FWHM. The sky signal is made of the CMB and the three major diffuse foreground emissions, namely synchrotron, free-free and dust. Their contribution has been derived using the following models. The CMB template varies in the MC chains, corresponding to Gaussian realizations of the theoretical no running best fit CMB angular power spectrum from $WMAP$[3] obtained with the `cmbfast` code (Seljak & Zaldarriaga 1996). We have verified that up to $\ell \lesssim 400$, which are the scales of interest for $1°$ smoothed data, differences between 3yr and 1yr best-fit model are less than 1.5%. For synchrotron, we use the all sky template at 408 MHz by Haslam et al. (1982); note that this does not include the extension by Giardino et al. (2002) on sub-degree angular scale in total intensity and polarization following the data in the radio band (Jonas et al. 1998; Reich & Reich 1986; Duncan et al. 1999; Uyaniker et al. 1999). For the dust, the 100 μm map by Finkbeiner et al. (1999) has been used; the free-free template is derived assuming correlation with the H_α emission (Finkbeiner 2004). These templates have been scaled to $WMAP$ frequencies assuming the weights given in Table 4 of the work by Bennett et al. (2003b). The sky maps are treated following the HEALPix sphere pixelization scheme[4] at $N_{side} = 512$ resolution parameter corresponding to about 7 arcminutes pixels. Our foreground model is based on 1-year $WMAP$ results. A more realistic approach to foreground emissions could use either the K-Ka template for "synchrotron" emission or the 3-year MEM foreground results (Hinshaw et al. 2006). However the use of these maps introduces subtleties mainly related to the noise in the data. Although the K-Ka map is likely a superior tracer of the synchrotron emission than Haslam at $WMAP$ frequencies, for our demonstration purposes the model used is sufficient.

The complete pipeline considered is therefore based on the following steps:

 (i) simulating CMB sky according to the $WMAP$ best-fit model convolved with the channel-specific beams;
 (ii) adding foreground emission scaled to each frequency band using the $WMAP$ weights specified above;
 (iii) adding noise realizations according to the sensitivity maps provided by the $WMAP$ team;
 (iv) deconvolving the beam and smooth to $1°$ FWHM each frequency channel simulation;
 (v) applying FASTICA on the simulated set of maps.

From each simulation we collect the results building figures of merit both on the full-sky and excluding Galactic plane regions with the Kp2 mask, used by the $WMAP$ team for their CMB analysis and described in Bennett et al. (2003b).

---

[3] http://lambda.gsfc.nasa.gov/data/map/powspec/wmap_lcdm_pl_model_yr1_v1.txt
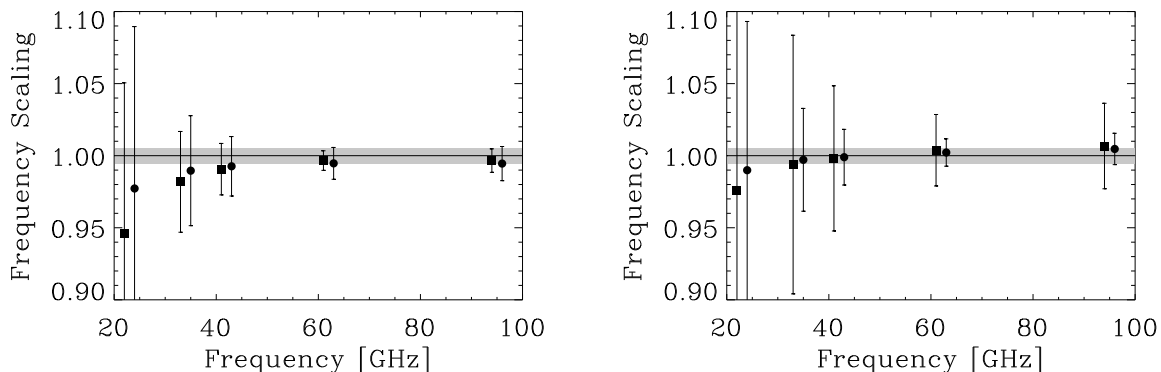[4] http://healpix.jpl.nasa.gov

Figure 1. ICA reconstructed CMB frequency scalings derived from 100 MC simulations. Boxes and circles represent full sky and Kp2 scalings respectively. The left (right) panel shows ideal results for noiseless (noisy) simulations. Also shown are the expected CMB frequency scaling and the 1-σ error (gray band) from the $WMAP$ analysis (Bennett et al. 2003a).

3.2 Simulations results and performances

From these set of simulations we derived the distributions for the CMB frequency scaling in each frequency band. This is obtained by taking the sum of the elements in the row of the **W** matrix which corresponds to the extracted CMB signal and multiply this by the corresponding column in the **A** matrix. Anticipating what we have done on real data, we also considered different combinations of $WMAP$ frequency bands with the aim of finding the optimal one for what concerns the CMB reconstruction. Such combinations are: QVW, KaQVW, KQVW, KQV, KaQV, KKaQV and KKaVW. Figure 1 shows results for the CMB frequency scalings reconstructed by ICA for noiseless (left panel) and noisy (right panel) simulations for both the full-sky (filled box) and Kp2 (filled circles) analysis for the KKaQVW combination. The agreement with a pure black-body spectrum (thick horizontal line) is quite good and almost within 1-σ limit of $WMAP$ calibration accuracy: low frequency channels (K and Ka bands) show larger uncertainties while if the bands considered are those where the CMB is stronger, the reconstruction is much more faithful. The error bars in the figure are purely indicative of the expected performance of ICA on the real data by $WMAP$. Indeed, the foregrounds are far too simple to accurately represent their real signal in the microwave band, at least for the low frequency components, synchrotron and free-free, where observations are limited in angular resolution, or indirect. Other unknowns are represented for example by the spatial variation of the frequency spectral index. Nevertheless the shown error bars give a flavor of the kind of accuracy of the results we show in the next Section. In addition, since for simulations we know exactly the input CMB sky, we evaluate both the average and the rms of the residual map obtained subtracting the CMB input and output. We also consider noiseless simulations in order to check the impact of the instrumental noise on the quality of the reconstruction. In the upper left panel of Figure 2 we show the average residual map from 100 simulations using all $WMAP$ channels in the ideal noiseless case: FASTICA removes the foregrounds to the level indicated in the figure, in units of thermodynamical temperature, with the strongest residual signal along the plane where the Galaxy is brighter. This is indeed expected since along the plane foreground emissions are expected to be correlated, violating one of the FASTICA assumptions. The peak-to-peak amplitude of the residual is around 8μK. Excluding Galactic plane regions and point sources with the Kp2 mask reduces sensibly the contamination (upper-right panel) down to $\sim 5\mu$K. Adding instrumental noise (lower-left) slightly decreases the quality of the reconstruction: the residuals are still present along the galactic plane and structures related to the actual noise distribution in the sky appear. Although quite similar between the $WMAP$ channels, the non-uniform noise distribution is interpreted by the algorithm as an additional "signal" component. However the peak-to-peak residual remains quite small being around 10.8μK. Finally in the lower-right panel we show the standard deviation of the residual map: the largest deviations are again along the Galactic plane where a very bright spot is clearly visible at a level of 20μK. However for the Kp2 analysis the overall rms decreases to less than 6 μK indicating a good quality in the FASTICA reconstruction; the scanning pattern of $WMAP$ is also evident.

Simulations here include only four signal components to be extracted with five frequency channels, and in the actual implementation the FASTICA tries to recover a number of components equal to the one of the frequency channels considered; also we do not know a priori the order in which components are extracted. Adopting a criterion already used in previous works (Maino et al. 2003), we were able to verify that the fifth component is clearly not physical, evaluating its signal-to-noise ratio; however its small amplitude slightly contaminates the other extracted components, and the best configuration for FASTICA is with four frequency channels at least in simulations. The situation is slightly different in the application to $WMAP$ real data due to the physical properties of real foregrounds.
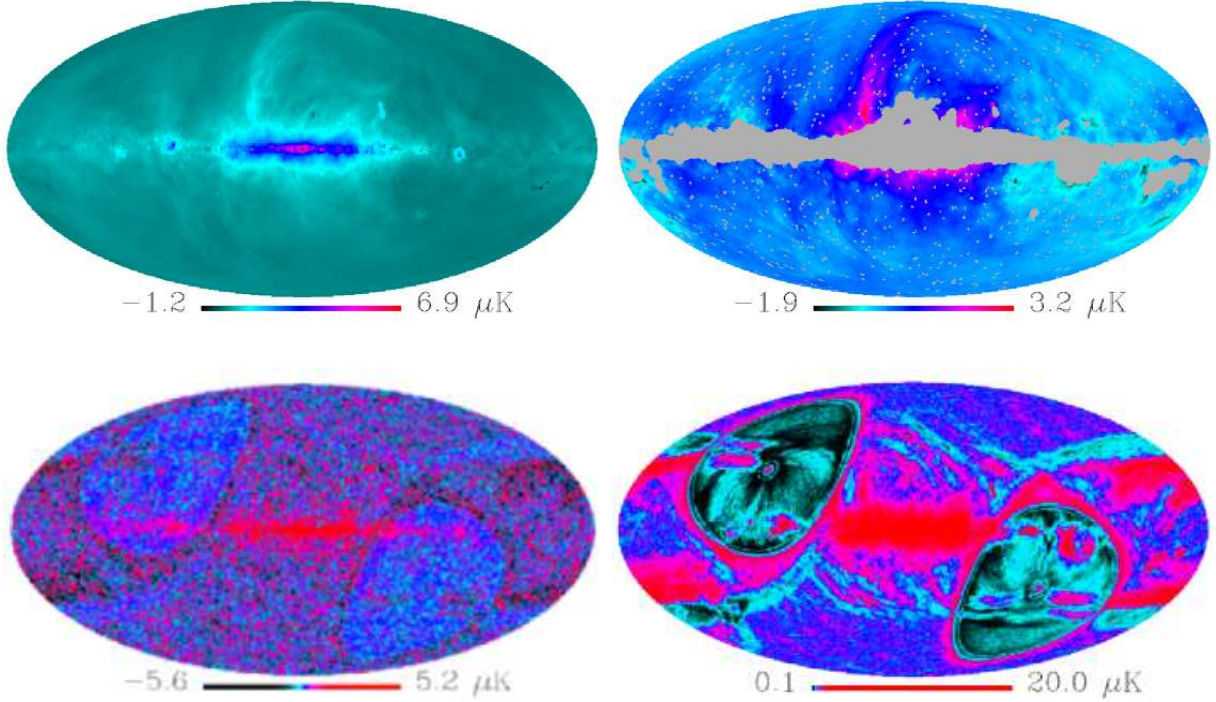
Figure 2. Maps of the average and standard deviation of the difference between reconstructed and input CMB maps. Each map is computed for a total of 100 simulations. The upper panels show the residual average for the ideal noiseless case when the reconstruction is done on the whole sky (left) and excluding the regions inside the Kp2 mask (right). The lower-left panel shows the residual average for the full-sky analysis with instrumental noise. The lower-right panel shows the standard deviation of the residual maps for full-sky and noisy case.

4 APPLICATION TO *WMAP* 3YR DATA

In this Section we show the results obtained by applying the FASTICA algorithm to the *WMAP* data. There are three main findings and criteria, namely the combination of the different *WMAP* channels, the results for the power spectrum and the distribution of the CMB power as recovered by the FASTICA across the sky, which are the subjects of the following sub-sections.

4.1 Selection of input maps

FASTICA operates onto the *WMAP* 3yr data smoothed at 1 degree FWHM at $N_{\mathrm{side}} = 512$, on the full sky and using the Kp2 mask. It is interesting to study the results for several combinations of the *WMAP* channels, selecting in particular the optimal one for what concerns the CMB reconstruction. We have performed our analysis considering the whole set of *WMAP* data as well as suitable subsets thereof. In particular we have set the minimum number of input channels to three taking the following combinations: QVW, KQVW, KaQVW, KQV, KaQV, KKaQV and KKaVW. The first three include high frequency CMB dominated channels: the rationale of adding to QVW the data in K or in Ka band is to provide the FASTICA dataset with a frequency band where the low frequency foregrounds dominate to better assess and remove the corresponding contamination to the CMB, and to check which between the K and Ka bands is more representative of such contamination. The next three sets exclude the W band data in order to see which channel dominates the CMB reconstruction, while the final one is included since the final *WMAP* 3-yr CMB angular power spectrum for $\ell > 12$ has been obtained by combining V and W bands data after subtraction of the K-Ka map plus free-free and dust templates. Several things have to be noted.

First all the recovered full-sky CMB maps show clearly a residual contamination along the galactic plane; we report in Fig. 3 the FASTICA CMB reconstruction from the KKaQVW combination as well as the difference between this map and the corresponding one from the Kp2 analysis.

The Galactic residual contamination is due to the fact that along the plane the foreground emissions are expected to be correlated, violating one of the FASTICA assumptions, as it was already evident in the simulations in the previous Section, although in that case the effect is much smaller in amplitude. This is an indication of the fact that our sky model is too far simple to properly reproduce the case with real data. This issue could be solved in principle by using a sort of Internal Template approach as exploited by Hansen et al. (2006) and currently under study (Stivoli et al. 2006b). In the difference

Table 1. FASTICA weights for different channels combination

K	Ka	Q	V	W
		Full-sky		
0.001610	0.039723	-0.932632	2.02027	-0.128972
-	-	-0.832358	1.93718	-0.104825
0.002866	-	-0.849484	1.94972	-0.102067
-	0.007923	-0.947255	1.93514	-0.095834
-0.026772	0.104729	-0.872566	1.79461	-
-0.008567	-	-0.755391	1.76396	-
-	-0.034631	-0.730927	1.76556	-
0.108010	-0.680878	-	1.64439	-0.071519
		Kp2 sky cut		
-0.183053	0.248303	-0.158422	0.767720	0.325453
-	-	-0.810260	2.231690	-0.421430
-0.148842	-	0.232536	0.748460	0.167486
-	-0.573262	0.524846	1.23660	-0.188187
0.074617	-0.413025	-0.327681	1.66609	-
0.001962	-	-0.750511	1.74855	-
-	-0.436905	0.295693	1.14121	-
-0.508637	1.18968	-	-0.703798	1.02276
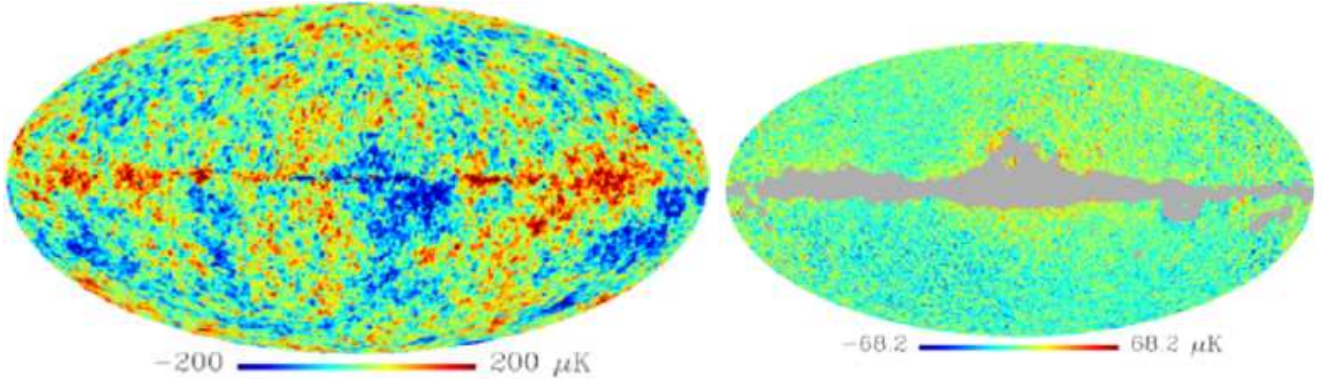
Figure 3. Left - CMB ICA map for full sky KKaQVW analysis. The residual along the Galactic plane is evident. Right - Difference between full sky and Kp2 ICA CMB maps: some residual Galactic signals is present near the edge of the sky mask and around some bright sources. High latitudes, large scale residual patterns are also present.
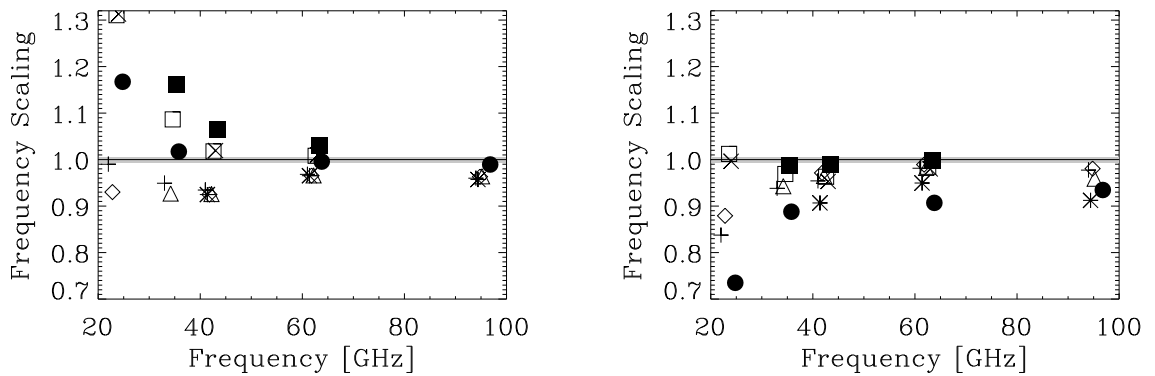
Figure 4. CMB frequency scaling for full-sky (left panel) and Kp2 analysis (right panel). Plus signs refer to KKaQVW combination, asterisks to QVW, rombs to KQVW, triangles to KaQVW, empty square to KKaQV, crosses to KQV, filled squares to KaQV and filled circles to KKaVW.

map large residuals are mainly located near the edge of the sky mask and around bright point sources: this is not surprising as we will see shortly. Moreover large scale residual is also present and we will comment on this when considering power spectrum analysis.

In addition we report in Fig. 4 FASTICA reconstructed CMB frequency scalings for both full-sky (left panel) and Kp2 sky cut (right panel) analysis. The improvement in the reconstruction when working with the Kp2 mask is evident at least for the low frequencies (K, Ka and Q bands) but not marked. Indeed the two CMB dominated channels are closer to the expected scaling for the full sky analysis than when Kp2 mask is applied: deviations are clear for the QVW combination and particularly for KKaVW channels which are quite peculiar as we will see below. This indicates that these three channels (QVW) do not provide enough information to FASTICA on the low-frequency contamination to properly perform a CMB cleaning.

For what concerns the frequency scaling the optimal combination is the one with KQVW where the deviation from the expected value of 1 for the highest frequency channels is smaller. This is an interesting result: it indicates that according to the figure of merit adopted, the low foreground emission is better "read" by FASTICA by means of the information in the K-band which is then subtracted optimally in the Q, V and W ones. On the other hand, this maximum in the quality of the CMB reconstruction lies in a plateau, in the sense that the results for other combinations are stable and pretty consistent with each other, as the rest of the analysis shows.

In Table 1 we also report the FASTICA weights for the different channel combinations and sky cuts. It may be immediately noted that the number variation is macroscopic, even within a given case, either on the full sky or outside the Kp2 mask. Indeed, a different combination of the $WMAP$ channels implies a different relative distribution of the background and foreground components, making FASTICA converging to a different separation matrix. The difference in the dataset by selecting different channel combinations is enhanced by the fact that $WMAP$ foregrounds are real, e.g. they possess a space varying spectral index. On different combinations FASTICA deals with a different sky rather than the same one at different frequencies, making the problem and the solution markedly varying. Despite of this, the reconstructed CMB power spectrum is pretty consistent in the different cases, as we see in a moment, and some general trends are clearly visible. First of all the dominant component with respect to the weight amplitude is always V-band for both full sky and Kp2 analysis. This is not surprising since it has the lowest foreground contamination. Furthermore in full sky analysis Q-band has always large negative weights almost stable with respect to the different combinations and similarly to the W-band they are both stable and negative. The Kp2 analysis assigns again largest weights to the V-band, apart from the KKaVW combination, while the overall behaviour of the results is less stable possibly due to the difference in the sky that FASTICA has to deal in each case, due to the fact that the data are real in the present case. A possible trend is that when both K- and W-bands are included, the weights in K are positive while they are negative for W-band. This could be related to the fact that the W band traces dust possibly both thermal and anomalous component, and K presumably contains some anomalous dust too. We also verified that the same instability in the weights recovered by the FASTICA occurs considering the other masks provided by the $WMAP$ team (namely the Kp0 and the Kp2 extended mask). Specifically, keeping the channel combination fixed but varying the mask, the weights variation has roughly the same magnitude as in Table 1. The interpretation we give is the relevance of the foreground signal on the ridge of a given mask, where the foreground themselves are more intense. Changing the cut is equivalent to include or exclude areas where the foreground emission is intense, and most likely exhibits different properties, as expected for realistic astrophysical emissions. Thus FASTICA deals in each case with a different problem, with the result of finding different weights of the different channels which maximize the independence of background and foregrounds. This situation is clearly evident, as reported commenting the derived frequency scalings, for the KKaVW combination: W-band is almost left untouched while other frequencies combine to create the "foreground" map to be subtracted from the W-band data. This is completely different from the previous findings and it is another indication of what reported before: different combinations are indeed different skies to be analysed. In this specific case without Q-band and without the region near the galactic plane, FASTICA detects different signal statistics as demonstrated by the different weights obtained. However the quality of the CMB reconstruction is still quite good given the high statistical independence of CMB with respect foregrounds as reported in the following analysis on the power spectrum.

4.2   Power Spectrum

Here we derive the angular power spectrum from the ICA CMB maps discussed above using the MASTER algorithm (Hivon et al. 2002), restricting to the cases in which the Kp2 mask has been used. This means that we also consider the full sky results after applying the Kp2 mask. Noise biases are obtained from noise-only simulations of the $WMAP$ frequency channels, combined with derived ICA weights (see Table 1) specific of each channel combination considered.

The final $WMAP$ 3yr power spectrum have been estimated using a combination of a maximum-likelihood approach for multipoles $\ell < 12$ and a MASTER technique for higher multipoles. However since we adopt a MASTER approach also at low multipoles for a proper comparison we report here the full MASTER $WMAP$ 3yr power spectrum kindly provided by the $WMAP$ team (Hinshaw 2006). Figure 5 presents our results for the selected channel combinations compared to the $WMAP$ 3yr CMB power spectrum.
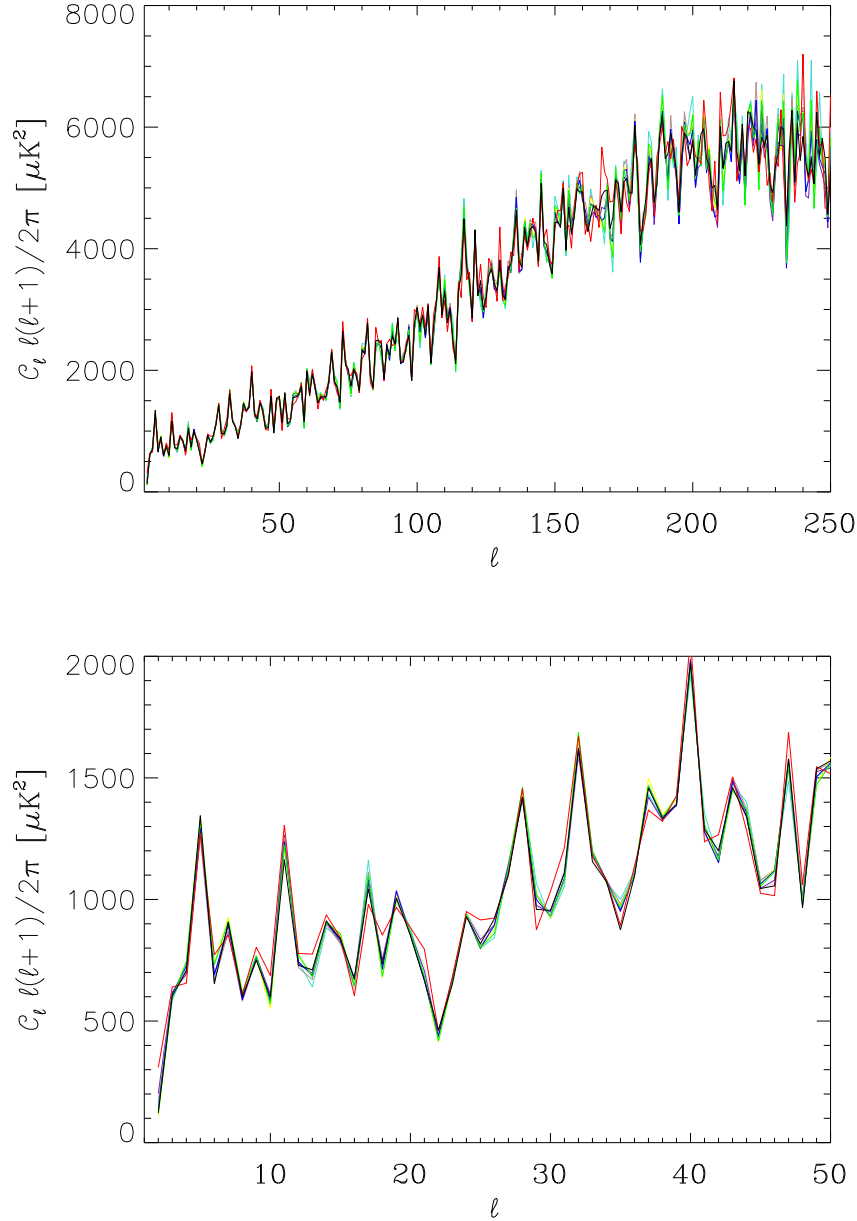
Figure 5. The power spectrum from all the $WMAP$ channel combinations on Kp2 compared with the full MASTER $WMAP$ 3yr power spectrum (black thick solid line). The top panel shows the analysis considering all multipoles, while the bottom panel reports results for low ℓs only, see text. Channel combinations are color coded: red for KKaQVW, green for QVW, blue for KQVW, yellow for KaQVW, brown for KKaQV, indigo for KaQV, turquoise for KQV and grey for KKaVW.

There is a complete consistency between the power spectra obtained from different channel combinations and the $WMAP$ 3yr results. The analysis on the low ℓ part of the spectrum shows again a general good agreement between ICA results and $WMAP$ 3yr data almost regardless of the channel combination considered. This is interesting since the $WMAP$ result has been obtained considering only high frequency channels after subtraction of foreground template as traced by the difference between low frequency channels. This result represents an indication of the high quality results that FASTICA can obtain in terms of CMB reconstruction on real CMB data.

We report in Figure 6 (upper panel) a similar comparison but for the binned power spectra and the agreement is evident both on the low multipoles as well as to higher ones up to $\ell \simeq 150$. Large spread in the results is present for the highest bins. Adopting the consistency with the $WMAP$ 3yr power spectrum as a figure of merit, we can judge which is the optimal combination: this is once again the KQVW, indicating that the best tracer of low frequency foreground contamination at high
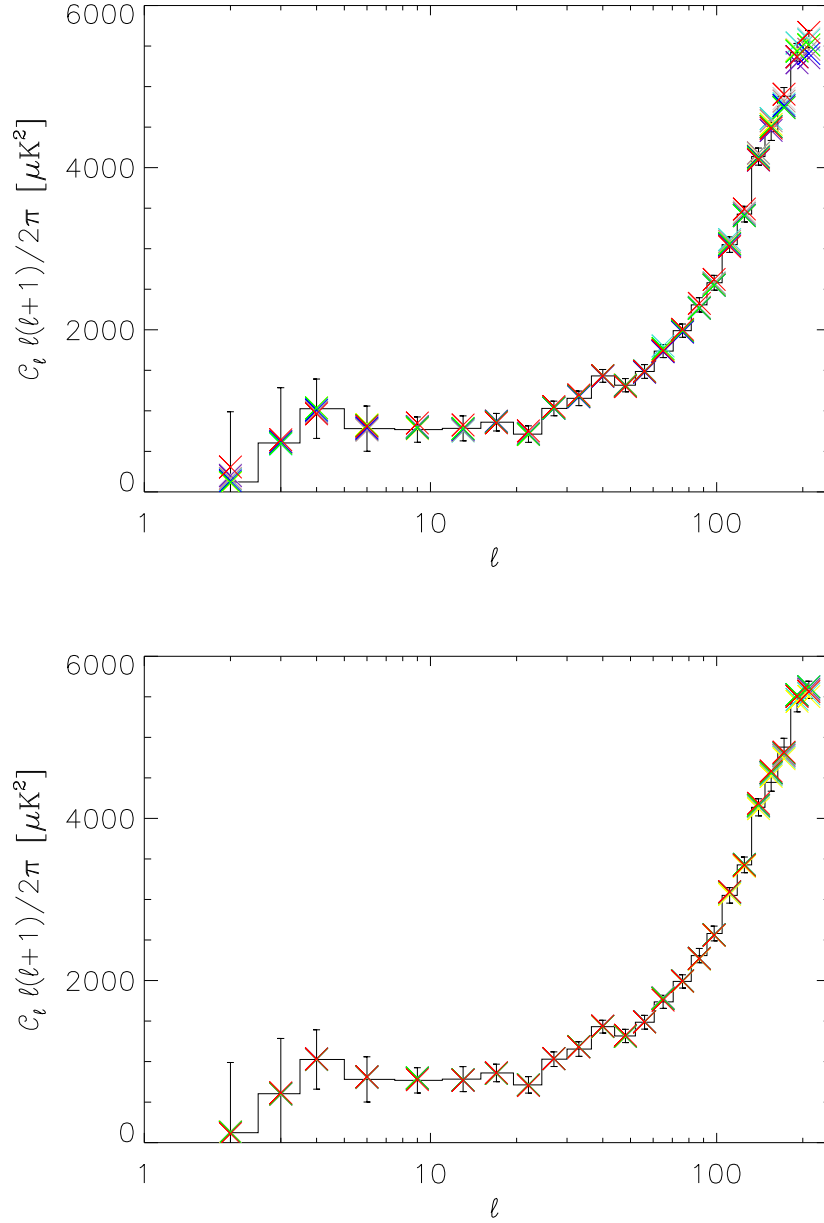
Figure 6. The binned power spectra from all *WMAP* channel combinations compared with the full MASTER *WMAP* 3yr power spectrum for a complete Kp2 analysis (upper panel) and full sky analysis with Kp2 mask applied when computing the power spectrum (lower panel). Channel combinations are color coded as in the previous figure.

frequencies is represented by the K band data. On the bottom panel we show similar results from the full sky analysis when the Kp2 mask has been applied: the agreement with *WMAP* results are even more evident for both low and high ℓ. This is an indication of the fact that even in presence of strong and possibly correlated foreground on the galactic plane, FASTICA is not only still able to properly recover the CMB pattern at high galactic latitudes but it performs better than in the case of a pure Kp2 analysis. This means that the level of signal correlation along the galactic plane, that violate one of the ICA assumptions, does not compromise the reconstruction at high galactic latitudes and that the regions near the plane included in the full sky analysis are useful for better distinguish different signal statistics.
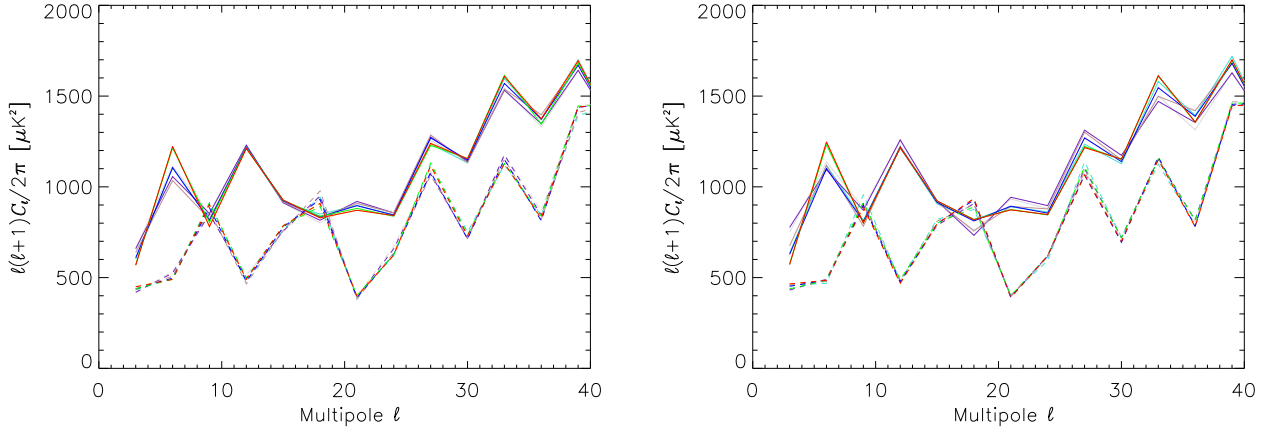
Figure 7. The power spectra derived on the northern (dashed line) and southern (solid line) hemisphere in the reference frame with north pole at $(\theta, \phi) = (80°, 57°)$. The left panel shows the spectra derived from the ICA CMB map out of Kp2. In the right panel the CMB maps are obtained applying FASTICA separately on the two hemispheres. Colors mark channel combinations as in previous figure.

4.3   Power Asymmetries

Given the quality of the results obtained so far especially when considering regions outside the Kp2 cut, we push the analysis further. Several authors (Eriksen et al. 2004b; Hansen et al. 2004, 2006), reported an unevenly distribution of large-scale power in the $WMAP$ 1yr data. The asymmetry is maximized in the direction defined by a north pole at $(\theta, \phi) = (80°, 57°)$ (Galactic co-latitude and longitude). Different and independent techniques found that in such reference frame the southern hemisphere has significantly more power than the northern hemisphere for $\ell < 40$. These findings have been confirmed in the $WMAP$ 3yr data. We therefore investigate the ICA CMB maps searching for this asymmetry.

As a first step, we computed the power spectrum on the ICA CMB maps, reconstructed out of Kp2, independently in the two hemispheres defined in the new reference frame. This is done for all the combinations of input frequency channels. The spectra are estimated in bins of 3 multipoles each from $\ell = 2 - 40$ and adopting the same procedure described in the previous Section. The results are shown in Fig. 7 (left panel). We can see that for all the channel combinations the southern spectrum has indeed more power than the northern one over almost the entire multipole range. We also performed the same kind of analysis starting from maps obtained from the full sky analysis and with Kp2 mask applied with identical findings. In a pure FASTICA analysis, one might be tempted to try an explanation in terms of a difference in the overall foreground spectral indices in the two hemispheres, since the FASTICA assumes an uniform frequency scaling across the whole sky; but the fact that other authors obtained the same result with totally independent procedures, and most importantly the test outlined below make this explanation unlikely. Indeed, we performed the component separation on the northern and southern hemisphere separately and derived the ICA CMB power spectrum separately for each of them. The spectra are reported in Fig. 7 (right panel). Also in this case the northern spectrum is systematically lower than the southern one. This result strongly disfavors an explanation based on foregrounds for the asymmetry found in the ICA CMB maps. In addition, we point out the remarkable agreement between our results and those of Hansen et al. (2006) (see their Fig. 8), obtained with a completely independent technique.

On the FASTICA side, this confirms the reliability of the algorithm when exploited to reconstruct the finest structure in the CMB pattern out of a given dataset, as this work and the previous ones on BEAST (Donzelli et al. 2006) and $COBE$-DMR (Maino et al. 2003) demonstrate; on a purely scientific side, we confirm the existence of a marked asymmetry in the CMB anisotropy power between the considered northern and southern hemispheres, which in this present case escapes explanations in terms of difference in the foreground properties on the corresponding two hemispheres.

5   CRITICAL DISCUSSION AND CONCLUSION

In this work we applied the fast Independent Component Analysis (FASTICA) component separation technique to the 3 years data of the Wilkinson Microwave Anisotropy Probe ($WMAP$). The algorithm retrieves the different components superposed in a multi-frequency observation as linear combinations of the input data at different frequencies, which maximize the mutual statistical independence. We first evaluate the expected performance by means of Monte Carlo chains on simulated $WMAP$ data varying the noise and CMB realization, and exploiting the existing foreground models. Among the recovered components, we identify one which is compatible with the CMB emission by checking the recovered frequency scaling. On

simulations, the precision of the recovery on the frequency scaling is of the order of percent. We then apply the technique to the real data, again identifying the CMB component by means of the reconstructed frequency scaling. Different combinations of the $WMAP$ channels give consistent results; in terms of the reconstruction of the CMB frequency scaling, the best $WMAP$ configuration includes the three high frequency channels (Q, V and W, respectively at 41, 61, 94 GHz), plus the lowest one (K at 23 GHz). This indicates that the algorithm benefits from having a good tracer of the low frequency foregrounds in the $WMAP$ data in order to achieve a proper CMB cleaning. The recovered CMB power spectrum is in close agreement with the $WMAP$ one on all accessible scales. The CMB fluctuation asymmetry in the northern and southern hemisphere claimed by several authors exploiting different data analysis techniques is confirmed in this work, with the same amplitude.

The agreement of the present results on CMB with the $WMAP$ ones and those from other authors is remarkable and strengthens the confidence we have on the CMB pattern reconstructed from the existing data as a whole. At the same time, from the point of view of the development of component separation techniques based on the Independent Component Analysis (ICA) this work represents the achievement of a most important milestone in view of the application to the Planck and other experiments; it means that the algorithm proved itself to be stable against the $WMAP$ instrumental systematics, and realistic foregrounds.

On the other hand, we are aware of the limitations of the present analysis. First of all, $WMAP$ is not an ideal experiment for performing a map based component separation, since the different channels have markedly different resolutions, and one has to do a pre-processing step decreasing the angular resolution of the data to a common one, which is about 1 degree in the present case. Second, the precision of the separation is evaluated by means of Monte Carlo chains on simulated data, which rely on ingredients, e.g. foregrounds and systematics, which may be far from reality, and also incomplete in the case of $WMAP$, as the dust foreground is visible only in the W band at 94 GHz, and does not have a multi-frequency coverage required by most component separation algorithms.

Despite of all these oddities, the CMB pattern recovered by the FASTICA is consistent with the results in earlier literature, and confirms effects like the asymmetric distribution of the CMB anisotropy power across the sky. This performance is likely to be due to the high level of statistical independence between background and foregrounds in the data, which is able to drive the solution close to the right one even for data affected by instrument systematics and realistic foregrounds. Thus we believe the present technique might be proving itself useful for future CMB probes, either accessing the CMB statistics beyond the power spectrum, and to control the foreground emission in polarization, which is going to be less known than in total intensity, and substantially higher compared with the CMB.

REFERENCES

Amari S., Chichocki A., 1998, *Proc. IEEE* , 86, 2026
Baccigalupi C. et al. , 2000, *MNRAS* , 318, 769
Baccigalupi C., 2003, *New Astron. Rev.* , 47, 1127
Baccigalupi C. et al. , 2004, *MNRAS* , 354, 55
Barreiro R.B. et al. , 2004, *MNRAS* , 351, 515
Bennett C.L. et al. , 2003a, *Astrophys. J. Supp.* , 148, 1
Bennett C.L. et al. , 2003b, *Astrophys. J. Supp.* , 148, 97
Bouchet F.R., Prunet S., Sethi S.K., 1999, *MNRAS* , 302, 663
Brandt W.M., Lawrence C.R., Readhead A.C.S., Pakianathan J.N., Fiola T.M, 1994, *Astrophys. J.* , 424 1
Copi C.J., Huterer D., Schwarz D.J., Starkman G.D., 2006, submitted to *Phys. Rev. D* , preprint available at
  `arXiv.org/abs/astro-ph/0605135`
Delabrouille J., Cardoso, J.F., Patanchon, G., 2003, *MNRAS* , 346, 1089
Donzelli S. et al. , 2006, *MNRAS* , 369, 441
Duncan A.R., Reich P., Reich W., Fürst E., 1999, *Astron. & Astrophys.* , 350, 447
Eriksen H.K., Hansen F.K., Banday A.J., Górski K.M., Lilje P.B., 2004a, *Astrophys. J.* , 605, 14
Erisken H.K., Banday A.J., Górski K.M., Lilje P.B., 2004b, *Astrophys. J.* , 612. 633

Eriksen H.K. et al. , 2006, *Astrophys. J.* , 641, 665

Finkbeiner D.P., Davis M., Schlegel D.J, 1999, *Astrophys. J.* , 524, 867

Finkbeiner D.P., 2004, *Astrophys. J.* , 614, 186

Giardino G. et al. , 2002, *Astron. & Astrophys.* , 387, 82

Górski K.M. et al. , 2005, *Astrophys. J.* , 622, 759

Hansen F.K., Banday A.J., Górski K.M., 2004, *MNRAS* , 354, 641

Hansen F.K., Banday A.J., Erisken H.K., Górski K.M., Lilje P.B, 2006, *Astrophys. J.* , submitted

Haslam C.G.T. et al. , 1982, *Astron. & Astrophys. Suppl.* , 47, 1

Hinshaw G. et al. 2003, *Astrophys. J. Supp.* , 148, 135

Hinshaw G. et al. 2006, *Astrophys. J.* , submitted

Hinshaw G., 2006, private communication

Hivon E. et al. , 2002, *Astrophys. J.* , 567, 2

Hyvärinen A., 1999, *IEEE Signal Processing Lett.* , 6, 145

Hyvärinen A. & Oja E., 2000, *Neural Networks* , 13, 411

Hobson M.P., Jones, A.W., Lasenby A.N., Bouchet F., 1998, *MNRAS* , 300,1

Jonas J.L, Baart E.E., Nicolson G.D., 1998, *MNRAS* , 297, 977

Kovac J. et al. , 2002, *Nature* , 420, 772

Maino D. et al. , 2002, *MNRAS* , 334, 53

Maino D., Banday A.J., Baccigalupi C., Perrotta F., Górski K.M., 2003, *MNRAS* , 344, 544

Montroy T. et al. , 2005, submitted to *Astrophys. J.* , preprint available at `arXiv.org/abs/astro-ph/0507514`

Page L. et al. , 2006, submitted to *Astrophys. J.* , preprint available at `arXiv.org/abs/astro-ph/0603450`

Patachon G., Cardoso, J.F., Delabrouille, J., Vielva P., 2005, *MNRAS* , 364, 1185

Reich P. & Reich W., 1986, *Astron. & Astrophys.* , 339, 187

Seljak U., Zaldarriaga M., 1996, *Astrophys. J.* , 469, 437

Spergel D.N. et al. , 2006, submitted to *Astrophys. J.* , preprint available at `arXiv.org/abs/astro-ph/0603449`

Stivoli F., Baccigalupi C., Maino D., Stompor R., 2006, *MNRAS* , in press

Stivoli F. et al. , 2006b, in preparation

Stolyarov V., Hobson M.P., Lasenby A.N., Barreiro R.B., 2005, *MNRAS* , 357, 145

Tegmark M., Efstathiou G., 2006, *MNRAS* , 281, 1297

Uyaniker B., Fürst E., Reich W., Reich P., Wielebinski R., 1999, *Astron. & Astrophys. Suppl.* , 138, 31